Experimental Validation of Zero Padding in SEFDM Systems Using Over-the-Air Transmission

Waseem Ozan, Ryan Grammenos and Izzat Darwazeh
Department of Electronic and Electrical Engineering, University College London, London, UK, WC1E 6BT
{w.ozan; r.grammenos; i.darwazeh}@ucl.ac.uk

***Abstract*—Non-orthogonal spectrally efficient frequency division multiplexing (SEFDM) saves bandwidth by compressing the frequency spacing between the subcarriers. This is at the cost of introducing inter-carrier interference (ICI) between the subcarriers. This self-created ICI compounded by the signal degradation caused during wireless propagation in multipath environments, complicates the task of channel estimation and equalisation. Recent studies suggest that combining zero padding (ZP) with SEFDM signals can simplify the challenge of channel estimation and equalisation in the frequency-domain. In this work, we validate experimentally the new ZP scheme through over-the-air transmission of radio frequency (RF) signals. Experimental results prove that using ZP in SEFDM enhances the channel estimation and equalisation accuracy, in comparison to conventional cyclic prefix (CP)-SEFDM. In addition, it is shown that ZP-SEFDM offers robustness against timing offsets.**

***Index Terms*—zero padding, guard interval, over-the-air transmission, experimental, non-orthogonal, spectrally efficient, SEFDM, channel estimation.**

I. Introduction

In order to mitigate the effect of inter-symbol interference (ISI) between adjacent multi-carrier symbols (in particular orthogonal frequency division multiplexing (OFDM)) in a multipath wireless channel, a guard interval is added to every transmitted symbol in the time-domain. This guard interval attached to each symbol can be (i) a copy of parts of the symbol, such as in cyclic prefix (CP) or (ii) a trail of zeros, such as in zero padding (ZP). A CP is generated by copying the last μ samples to the beginning of the symbol. On the other hand, ZP replaces the CP part by zeros attached to the end of each symbol. Fig. 1 depicts these two guard interval schemes, CP and ZP.

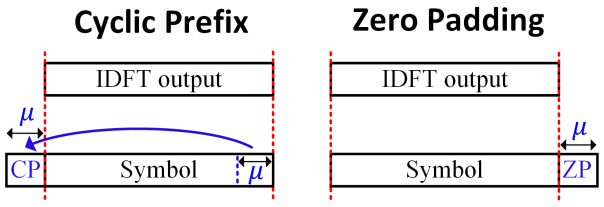

Fig. 1. Guard interval schemes for multi-carrier systems.

In 2002, the work by Muquet et al [1] provided a comprehensive evaluation for CP-OFDM and ZP-OFDM, which concludes that using ZP can enhance channel estimation and guarantee signal recovery. Ten years later, the debate of using either CP or ZP is extended to filter-bank multi-carrier systems (FBMC) [2], which shows that a circulant channel matrix can be obtained at the receiver by using either of the two guard interval schemes. The circulant matrix is diagonalised using a discrete Fourier transform (DFT), thus enables one-tap equalisation in the frequency-domain. Few years later, this debate of using ZP or CP was revisited in 2016 for OFDM [3], yet this time considering the use of filtering or windowing to improve spectral performance required in fifth generation (5G) communication systems. More recently, the work in [4], [5] propose the use of ZP instead of CP in spectrally efficient frequency division multiplexing (SEFDM). SEFDM is a non-orthogonal system, in which, the subcarriers are separated with frequency spacing that is below the orthogonality limit, to enhance the bandwidth utilisation with respect to OFDM. However, this leads to inter-carrier interference (ICI) among the subcarriers [6]. Hence, the received signal is affected by the self-induced ICI combined with multipath effects. Therefore, channel estimation and equalisation becomes more challenging in comparison to OFDM systems [7]–[11].

The work in [4], provides a comprehensive study of the trade-offs associated with the use of a CP versus ZP in SEFDM systems and concludes that ZP-SEFDM outperforms CP-SEFDM in terms of error rates. Also, the work proves analytically that using ZP in SEFDM decomposes the wideband channel into a number of orthogonal narrowband subchannels [4]. This enables the use of a one-tap equaliser in the frequency-domain at the receiver [4], [5]. However, the evaluation of ZP versus CP in SEFDM systems has been carried out using computer simulations only, which lacks the realistic communication signal impairments in radio frequency (RF) systems. Such impairments are timing offsets and multipath effects.

In this work, we validate experimentally the new ZP-SEFDM scheme using over-the-air transmission of RF signals. In addition, the paper presents a full study and investigation of ZP-SEFDM against the conventional CP-SEFDM scheme in terms of (i) channel estimation accuracy, (ii) system bit error rate (BER) performance and (iii) robustness to timing offsets.

The rest of the paper is organised as follows: Section II outlines the signal modelling and representation of ZP-SEFDM and CP-SEFDM; The SEFDM system operation is described in Section III; The experimental testbed specifications are detailed in Section IV; In Section V, the performance of ZP-SEFDM is compared against CP-SEFDM; Section VI concludes our paper.

II. Signal Representation of ZP-SEFDM and CP-SEFDM

The signal model for SEFDM is given in Section II-A. The signal representation and modelling of the CP-SEFDM scheme is provided in Section II-B, while ZP-SEFDM is described in Section II-C.

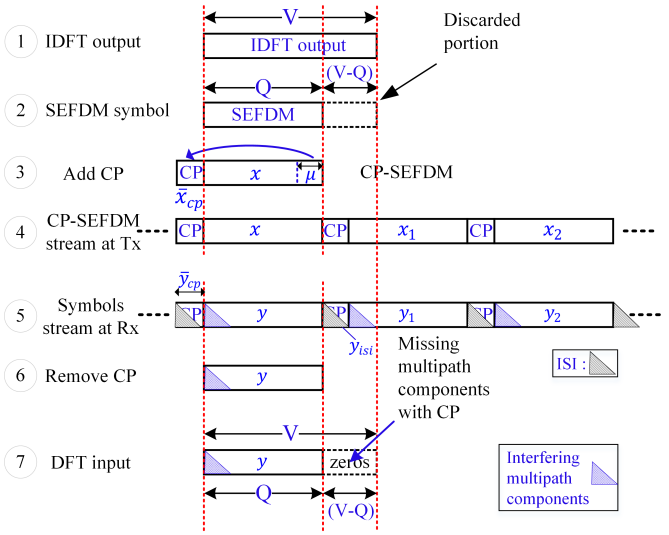

Fig. 2. Signal structure representation for CP-SEFDM.

A. SEFDM Signal Model

SEFDM is a multi-carrier signal, which consists of N subcarriers, each modulated with a complex symbol. SEFDM saves signal bandwidth by $((1-\alpha) \times$ total bandwidth) in Hz, where α is the bandwidth compression factor, with reference to OFDM. An SEFDM symbol, $\mathbf{x} \in \mathbb{C}^{Q\times 1}$, is mathematically represented as:

$$x(k) = \frac{1}{\sqrt{Q}} \sum_{n=0}^{Q-1} s_n e^{\left(\frac{j2\pi\alpha nk}{Q}\right)} \tag{1}$$

where $k = [0, 1, 2, ..., Q-1]$ is the time sample index of the SEFDM symbol, $Q = \rho N$ is the total number of time samples, ρ is the oversampling rate and s_n is the complex symbol modulated on the n^{th} subcarrier.

B. CP-SEFDM

Fig. 2 illustrates the signal structure for CP-SEFDM. Steps 1 and 2 of the figure depict the inverse discrete Fourier transform (IDFT) output, the discarded part of this output and the SEFDM symbol. Step 3 of Fig. 2, depicts the generation of a conventional CP-SEFDM symbol, in which, the last $\mu \in \mathbb{N}$ samples of an SEFDM symbol, $\bar{\mathbf{x}}_{cp} \in \mathbb{C}^{\mu\times 1}$, are added to the beginning of this symbol. Unlike CP-OFDM symbols, CP-SEFDM symbols have phase discontinuity between the CP part and the SEFDM symbol, as shown in Fig. 3. The CP-SEFDM symbol is transmitted through a wireless frequency selective channel with channel impulse response (CIR) $\mathbf{h} = [h_0, h_1, \ldots, h_\mu] \in \mathbb{C}^{(\mu+1)\times 1}$.

At the receiver, the three signal parts, $\bar{\mathbf{y}}_{cp}, \mathbf{y}$ and $\mathbf{y}_{isi}$, are depicted in step 5 of Fig. 2; $\bar{\mathbf{y}}_{cp} \in \mathbb{C}^{\mu\times 1}$ is the CP part that is affected by the ISI components stemming from the previous SEFDM symbol and hence it is ignored at the receiver; $\mathbf{y} \in \mathbb{C}^{Q\times 1}$ is the received SEFDM symbol that is passed to the detection stage; $\mathbf{y}_{isi} \in \mathbb{C}^{\mu\times 1}$ represents the ISI components that are added to the succeeding SEFDM symbol. Having removed the CP, the demodulated CP-SEFDM symbol, $\tilde{\mathbf{r}}_{cp}$, is given as [4]:

$$\tilde{\mathbf{r}}_{cp} = \boldsymbol{\lambda} \odot \tilde{\mathbf{s}} + \tilde{\mathbf{r}}_{cp2} - \tilde{\mathbf{r}}_{cp3} + \tilde{\mathbf{z}}_{cp} \tag{2}$$

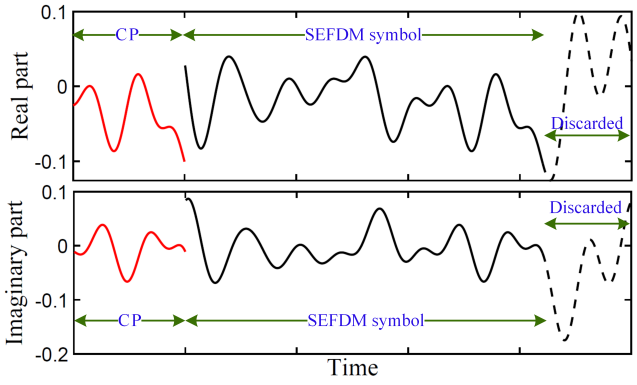

Fig. 3. Time samples of the real and imaginary parts of one CP-SEFDM symbol. The red parts constitute the guard interval while the black parts represent the IDFT output. The solid-black parts are the SEFDM symbols while the dashed-black parts are the discarded samples at the output of the IDFT.

where $\boldsymbol{\lambda}$ is the subchannel gains vector that provides the phase and amplitude gain/distortion at each subcarrier, $\tilde{\mathbf{s}} = \boldsymbol{\Gamma}\mathbf{s}$ is the expected received SEFDM symbol when no multipath or noise channels are present, $\boldsymbol{\Gamma} = \boldsymbol{\Phi}^H\boldsymbol{\Phi}$ is the correlation matrix, which provides the interference coefficients for each subcarrier from its neighbouring subcarriers [12], the element $\tilde{\mathbf{z}}_{cp}$ is the AWGN noise vector, and the notation $(\odot)$ is the element-wise multiplication. It should be evident that even in the absence of noise, the demodulated CP-SEFDM signal would comprise interference components from the missing and unwanted signals, $\tilde{\mathbf{r}}_{cp2}$ and $\tilde{\mathbf{r}}_{cp3}$, respectively.

Channel Estimation and Equalisation in CP-SEFDM: The CP-SEFDM analytical expression of channel estimation is found using zero forcing and it is given by [4]:

$$\begin{aligned}\hat{\boldsymbol{\lambda}} &= \tilde{\mathbf{r}}_{cp}./\tilde{\mathbf{s}} = (\boldsymbol{\lambda} \odot \tilde{\mathbf{s}} + \tilde{\mathbf{r}}_{cp2} - \tilde{\mathbf{r}}_{cp3} + \tilde{\mathbf{z}}_{cp})./\tilde{\mathbf{s}} \\ &= \underbrace{\boldsymbol{\lambda}}_{1} + \underbrace{\tilde{\mathbf{r}}_{cp2}./\tilde{\mathbf{s}}}_{2} - \underbrace{\tilde{\mathbf{r}}_{cp3}./\tilde{\mathbf{s}}}_{3} + \underbrace{\tilde{\mathbf{z}}_{cp}./\tilde{\mathbf{s}}}_{4}\end{aligned} \tag{3}$$

while the analytical expression of channel equalisation for CP-SEFDM is found using a one-tap equaliser and is given as:

$$\begin{aligned}\hat{\mathbf{r}}_{cp} &= \tilde{\mathbf{r}}_{cp}./\boldsymbol{\lambda} = (\boldsymbol{\lambda} \odot \tilde{\mathbf{s}} + \tilde{\mathbf{r}}_{cp2} - \tilde{\mathbf{r}}_{cp3} + \tilde{\mathbf{z}}_{cp})./\boldsymbol{\lambda} \\ &= \underbrace{\tilde{\mathbf{s}}}_{1} + \underbrace{\tilde{\mathbf{r}}_{cp2}./\boldsymbol{\lambda}}_{2} - \underbrace{\tilde{\mathbf{r}}_{cp3}./\boldsymbol{\lambda}}_{3} + \underbrace{\tilde{\mathbf{z}}_{cp}./\boldsymbol{\lambda}}_{4}\end{aligned} \tag{4}$$

where part 1 represents the subchannel gain $\boldsymbol{\lambda}$ estimated at each subcarrier in (3) and the desired signal $\tilde{\mathbf{s}}$ in (4), parts 2 and 3 are the added interference and part 4 corresponds to the noise signal. The division operator notation $(./)$ between the two vectors is the element-wise division.

C. ZP-SEFDM

In ZP-SEFDM, each transmitted SEFDM symbol, $\mathbf{x}$, is padded with zeros instead of appending a CP at the beginning of the SEFDM symbol. The transmitted SEFDM symbol may then be represented as in steps 3 and 4 of Fig. 4. At the receiver, the SEFDM symbol is affected by the multipath and AWGN channels, and $\bar{\mathbf{y}}_{zp} \in \mathbb{C}^{\mu\times 1}$ is the ZP part that contains the energy spillage due to ISI. The received signal parts are shown in step

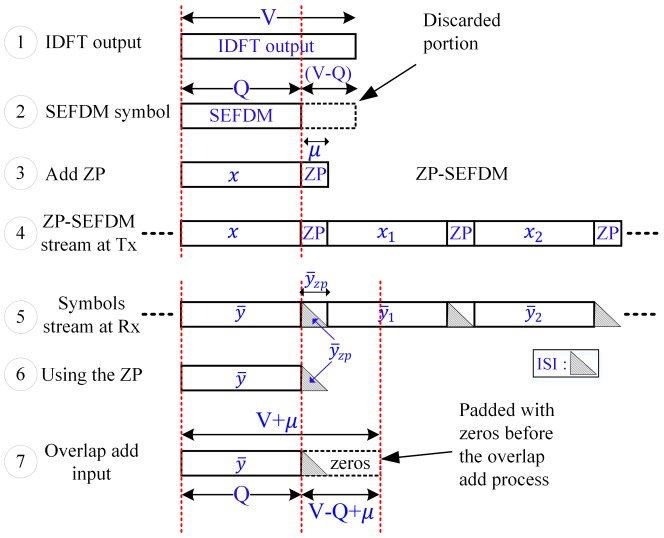

Fig. 4. Signal structure representation for ZP-SEFDM.

5 of Fig. 4. To determine the circulant channel matrix in ZP-SEFDM, the received SEFDM symbol, in which the ZP part carries ISI, is padded with zeros to length $V+\mu$, as shown in step 7 of Fig. 4. An overlap-add technique is then used before passing the symbol to an DFT [4]. The reason for using overlap-add is to design a general receiver for any value of α.

After that, the SEFDM symbols including the ZP part are fed to a DFT of size $V = Q/\alpha$. In this scenario, the demodulated signal, $\mathbf{r}_{zp}$, is expressed as [4]:

$$\mathbf{r}_{zp} = \boldsymbol{\lambda}_{zp} \odot \tilde{\mathbf{s}} + \tilde{\mathbf{z}}_{\Phi} \tag{5}$$

where $\boldsymbol{\lambda}_{zp}$ is the vector of subchannel phase and amplitude gain/distortion factors and $\tilde{\mathbf{z}}_{\Phi}$ is the noise vector. Equation (5), provides evidence that using ZP instead of a CP in SEFDM allows the decomposition of the wideband multipath channel into independent narrowband channels.

Channel Estimation and Equalisation in ZP-SEFDM: The analytical expression of estimated channel characteristics for ZP-SEFDM are given by:

$$\begin{aligned}\hat{\boldsymbol{\lambda}}_{zp} &= \mathbf{r}_{zp}./\tilde{\mathbf{s}} \\ &= (\boldsymbol{\lambda}_{zp} \odot \tilde{\mathbf{s}} + \tilde{\mathbf{z}}_{\Phi})./\tilde{\mathbf{s}} = \underbrace{\boldsymbol{\lambda}_{zp}}_{1} + \underbrace{\tilde{\mathbf{z}}_{\Phi}./\tilde{\mathbf{s}}}_{2}\end{aligned} \tag{6}$$

while the analytical expression of the equalisation process is given by:

$$\hat{\mathbf{r}}_{zp} = \mathbf{r}_{zp}./\boldsymbol{\lambda}_{zp} = \underbrace{\tilde{\mathbf{s}}}_{1} + \underbrace{\tilde{\mathbf{z}}_{\Phi}./\boldsymbol{\lambda}_{zp}}_{2} \tag{7}$$

where part 1 represents the subchannel gain $\boldsymbol{\lambda}_{zp}$ in (6) and the desired signal $\tilde{\mathbf{s}}$ in (7), while part 2 corresponds to the noise vector. The equations show that there is no additional interference due to the multipath channel. Unlike the case of CP-SEFDM in (4), equation (7) demonstrates that equalising the channel effects in ZP-SEFDM signals does not lead to additional interference between the subcarriers.

III. System Operation

Fig. 5 depicts a simplified SEFDM transceiver for system testing. In this scenario, the guard interval (GI) length is selected in accordance with the long-term evolution (LTE) standards [13]. The only difference is that the CP employed in LTE is replaced by ZP in this work.

As shown in Fig. 5, at the transmitter, a stream of bits, d, is generated and mapped into quadrature phase shift keying (QPSK) symbols to generate the data symbols, S. These symbols are input to an IDFT, which is used to generate the non-orthogonal SEFDM signal; where a specified number of zeros are appended to the input of the IDFT, thus giving rise to $V = Q/\alpha$ input samples. Consequently, a $V-$point IDFT is required to generate the SEFDM signal, of these V inputs N inputs are active subcarriers, with the remaining $V-N$ inputs are zeros. Now, out of these $V-N$ zeros, $(Q-N)$ zeros are introduced due to the ρ factor. The remaining $(V-Q)$ zeros which are added to the input of the IDFT depend on the α factor applied. The same number of $(V-Q)$ samples are discarded at the output of the IDFT, while the Q samples that are taken forward make up a single SEFDM symbol. This process may be understood better by referring to figures 2 and 4, specifically steps 1 and 2.

a) CP-SEFDM: The upper part of Fig. 5 depicts the CP-SEFDM system. Here, a CP, of length μ, is added to the beginning of every SEFDM symbol before the signal is transmitted through a wireless fading channel. Thus the number of time-domain samples of every transmitted SEFDM symbol is $Q+\mu$. At the receiver, the CP portion is discarded first and then, every SEFDM symbol is padded with zeros of length $(V-Q)$. The resulting signal is then fed to a DFT to convert the signal to the frequency-domain.

b) ZP-SEFDM: The lower part of Fig. 5 depicts the ZP-SEFDM system, in which the CP is replaced by trailing zeros of length μ that are attached to the end of each SEFDM symbol. The SEFDM symbols including the ZP arrive at the receiver distorted by the multipath channel and contaminated with AWGN; where the power within the ZP part is no longer equal to zero, due to the spillage of energy in the SEFDM symbols caused by the multipath channel. The SEFDM symbols plus the ZP portion are fed to the overlap-add process and its output of length V is passed to a DFT to convert the signal to the frequency-domain.

c) Overlap-Add process: The work in [4] proposes the use of the overlap-add process to allow the ZP-SEFDM scheme to be compatible with all the possible variations of the number of subcarriers, α and the ZP part length. The process is accomplished by padding the received SEFDM symbol and its ZP part with zeros to length $V+\mu$. After that, the last μ time samples are overlapped and added to the beginning of the received ZP-SEFDM symbol [4].

IV. Testbed Setup and Parameters

In this section we present the experimental software-defined radio (SDR) testbed that we used to evaluate the ZP-SEFDM system using over-the-air transmission. The testbed consists of a universal software radio peripheral (USRP) reconfigurable

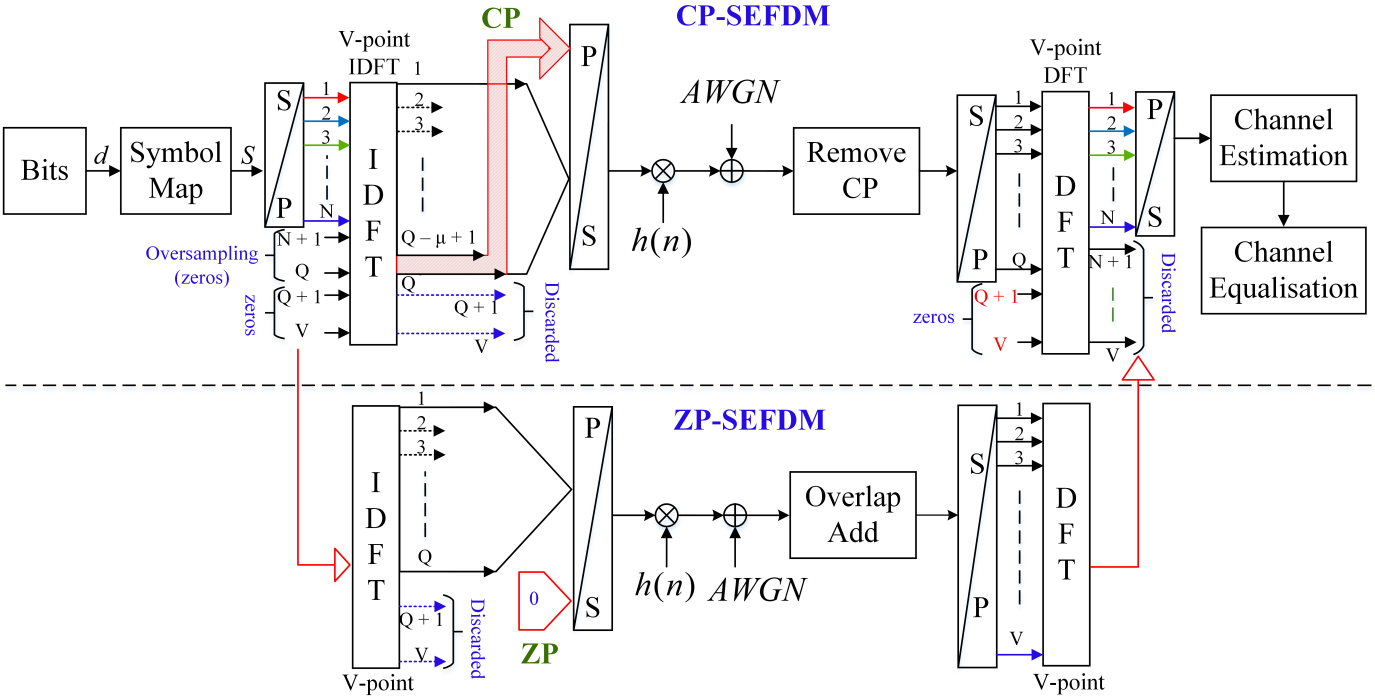

Fig. 5. Block diagram of a simplified SEFDM transceiver employing the proposed guard interval schemes. CP-SEFDM is represented in the upper part while ZP-SEFDM is represented in the lower part of the diagram.

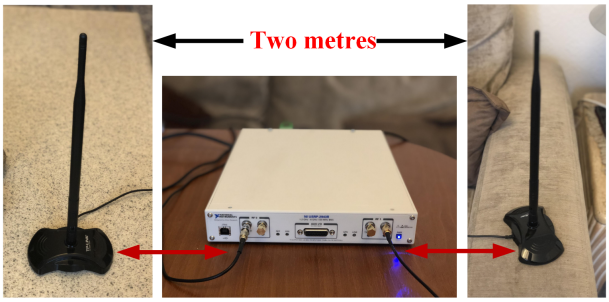

Fig. 6. Over-the-air transmission indoor testbed.

input-output (RIO) transceiver (National Instruments USRP-RIO 2943) programmed using LabVIEW NXG and a pair of TP-Link antennas. The signal processing blocks are implemented in LabVIEW NXG. A photograph of the experimental testbed is shown in Fig. 6.

The experimental system parameters are configured using the narrowband internet-of-things (NB-IoT) standard [14]. In order to accommodate the bandwidth compression factor α in NB-IoT systems, the standard parameters are appropriately modified following the work in [4], [15]. The system parameters are given in Table I.

The frame structure is similar to that in LTE [14] where the length of the radio frame is ten ms. Each frame consists of ten equally sized subframes, each of which comprise of 2×0.5 ms time slots. The number of SEFDM symbols in each time slot is seven symbols. One symbol out of these seven symbols carries a pilot, which is used for channel estimation, while the other six symbols convey data. For time synchronisation, the Schmidl and Cox technique is applied in this work [16].

TABLE I
EXPERIMENTAL SYSTEM SPECIFICATIONS

Parameters	Values
Central carrier frequency (GHz)	2
Sampling frequency (MHz)	1.92
Signal bandwidth (KHz)	$180\times\alpha$
Subcarrier baseband bandwidth (KHz)	15
Subcarrier spacing (KHz)	$15\times\alpha$
IDFT/DFT size	$\lceil 128/\alpha \rfloor$
Number of cyclic prefix samples	10
Number of data samples	128
Number of data subcarriers	12

V. System Performance Evaluation

The system under consideration is evaluated in terms of (*i*) mean square error (MSE), (*ii*) BER performance and (*iii*) timing offset.

A. MSE in channel estimation

The MSE is given by [4]:

$$\text{MSE} = \mathbb{E}\left\{[\boldsymbol{\lambda} - \hat{\boldsymbol{\lambda}}]^H [\boldsymbol{\lambda} - \hat{\boldsymbol{\lambda}}]\right\} \tag{8}$$

where $\boldsymbol{\lambda}$ is the gain of each subchannel under evaluation and $\hat{\boldsymbol{\lambda}}$ is the estimated subchannel gain measured at the receiver. The subchannels' gain, $\boldsymbol{\lambda}$, of the experimental over-the-air transmission is not available, and hence, computer simulations are used instead to assess the MSE performance for frequency-domain channel estimation. The computer simulation is carried out using 5G-new radio (5G-NR) tapped delayed line (TDL) channel model of type (D).

Fig. 7 compares the MSE of CP-SEFDM and ZP-SEFDM systems for two values of the compression factor, specifically $\alpha = 0.9$ and 0.7. The figure shows that, when CP-SEFDM fails to estimate the channel accurately resulting in high MSE values, the ZP-SEFDM scheme estimates well, for all values of E_b/N_o.

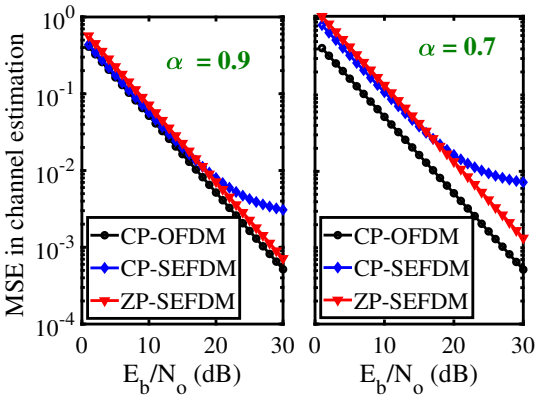

Fig. 7. MSE results using TDL-D channel model.

From the figure, it can be inferred that the MSE in channel estimation for CP-SEFDM systems eventually reaches a non-zero error floor for any value of $\alpha < 1$. On the contrary, the MSE for the ZP scheme is monotonically decreasing.

B. Practical BER performance

We measure the BER for a range of SNRs, as illustrated in Fig. 8. We use conventional CP-OFDM as the benchmark and compare the system performance of ZP-SEFDM and CP-SEFDM against this benchmark. In this work, the equalised complex data symbols are detected using a sphere decoder [6]. The experimental measurements are acquired through the over-the-air transmission of RF signals in an indoor multipath environment.

In equations (3) and (4), it was proved that using CP-SEFDM in a multipath environment, results in additional interference to the equalised symbols. This interference is a function of both the multipath effects and the compression factor, α, where the lower the value of α, the higher the interference added to the signal. This is evidenced in Fig. 8 wherein the BER performance of CP-SEFDM for $\alpha = 0.7$ degrades at high SNR values in comparison to ZP-SEFDM for the same value of α. This is due to the fact that the additional interference incurred in CP-SEFDM systems becomes more dominant with respect to the noise at higher SNR values. Therefore, the use of the proposed ZP scheme in SEFDM systems, improves the error rate in multipath environments for any value of α.

C. Timing offset assessment

It is a well-known fact that time synchronisation is more challenging in multipath environments [17], [18]. In conventional OFDM systems, a CP part is added to the beginning of each symbol to overcome this issue. Unlike CP-OFDM, however, CP-SEFDM presents phase discontinuity between the CP part and the start of the actual symbol, as depicted in Fig. 3. Therefore, a shift in the time samples results in additional interference between the subcarriers. The results of this timing offset are shown in Fig. 9, where CP-OFDM, CP-SEFDM and ZP-SEFDM are evaluated for different timing offsets using the over-the-air transmission testbed. From Fig. 9(a) it is clear that CP-OFDM has commensurate performance for different timing offsets. The same trends are shown for ZP-SEFDM, in that the measured BER is very similar for different timing offsets irrespective of the value of α, as indicated in Fig. 9(d) and Fig. 9(e). On the contrary, for CP-SEFDM systems, the error rate performance degrades with larger timing offsets, particularly for higher levels of bandwidth compression (lower values of α), as depicted in Fig. 9(b) and Fig. 9(c).

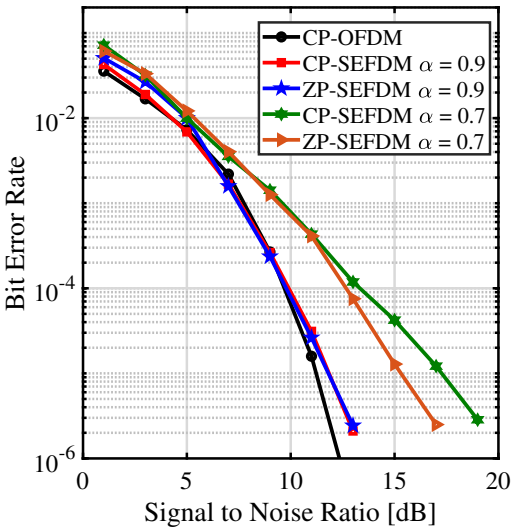

Fig. 8. Bit error rates for CP-OFDM, CP-SEFDM and ZP-SEFDM.

VI. Conclusion

In addition to the signal distortion caused by multipath channels, non-orthogonal multi-carrier systems (in particular SEFDM) also suffer from self-induced ICI. This complicates the task of channel estimation and equalisation processes. Recent studies suggest that using ZP instead of CP in SEFDM systems can enhance the accuracy of channel estimation and equalisation. In this work, the ZP-SEFDM scheme is validated experimentally using over-the-air transmission. Experimental evaluation show that ZP-SEFDM outperforms CP-SEFDM in terms of channel estimation and equalisation accuracy. Furthermore, the use of ZP in SEFDM systems improves robustness against timing offsets. This facilitates the practical implementation of SEFDM in future communication systems.

References

[1] B. Muquet *et al.*, "Cyclic prefixing or zero padding for wireless multi-carrier transmissions?" *IEEE Trans. Commun.*, vol. 50, no. 12, pp. 2136–2148, Dec 2002.

[2] F. Cruz-Roldán *et al.*, "Zero-padding or cyclic prefix for mdft-based filter bank multicarrier communications," *Signal Processing*, vol. 92, no. 7, pp. 1646–1657, 2012.

[3] S. Venkatesan and R. A. Valenzuela, "OFDM for 5G: Cyclic prefix versus zero postfix, and filtering versus windowing," in *Proc. IEEE Int. Conf. Commun. (ICC)*, May 2016, pp. 1–5.

[4] W. Ozan *et al.*, "Zero padding or cyclic prefix: Evaluation for non-orthogonal signals," *IEEE Communications Letters*, 2020.

[5] B. Yu *et al.*, "Channel equalisation and data detection for SEFDM over frequency selective fading channels," *IET Communications*, vol. 12, no. 18, pp. 2315–2323, 2018.

[6] I. Kanaras *et al.*, "Spectrally Efficient FDM Signals: Bandwidth Gain at the Expense of Receiver Complexity," in *Proc. IEEE Int. Conf. Commun.*, June 2009, pp. 1–6.

[7] S. Isam and I. Darwazeh, "Robust channel estimation for Spectrally Efficient FDM system," in *Proc. 19th Int. Conf. Telecommun. (ICT)*, April 2012, pp. 1–6.

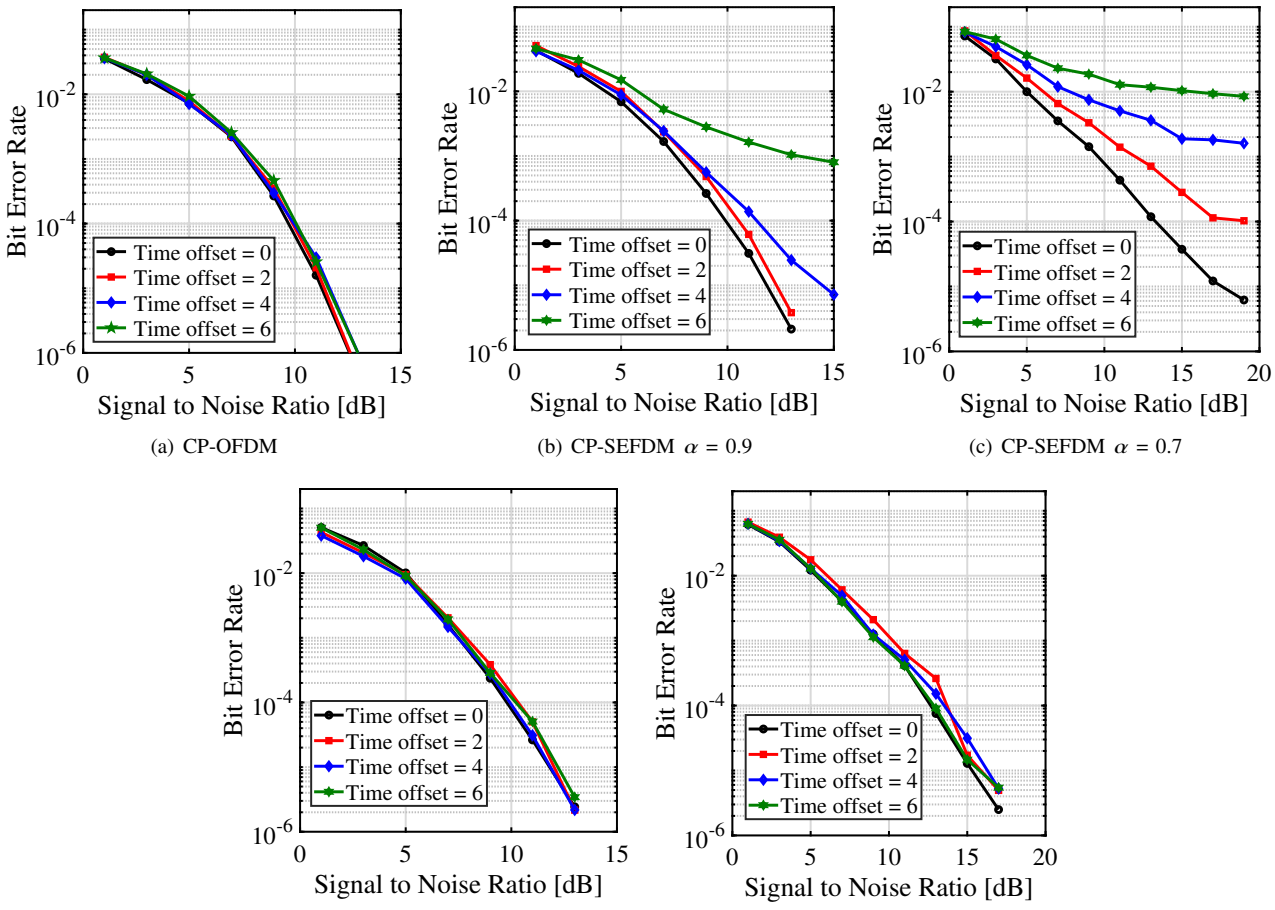

(a) CP-OFDM (b) CP-SEFDM $\alpha = 0.9$ (c) CP-SEFDM $\alpha = 0.7$

(d) ZP-SEFDM $\alpha = 0.9$ (e) ZP-SEFDM $\alpha = 0.7$

Fig. 9. Bit error rates for CP-OFDM, CP-SEFDM and ZP-SEFDM with $\alpha = 0.9$ and 0.7 and measured for different timing offsets. The unit of the timing offset is discrete time samples.

[8] W. Ozan *et al.*, "Experimental Evaluation of Channel Estimation and Equalisation in Non-Orthogonal FDM Systems," in *2018 11th International Symposium on Communication Systems, Networks & Digital Signal Processing (CSNDSP)*. IEEE, 2018, pp. 1–6.

[9] S. Gorbunov and A. Rashich, "BER performance of SEFDM signals in LTE fading channels," in *2018 41st International Conference on Telecommunications and Signal Processing (TSP)*. IEEE, 2018.

[10] Y. Mal *et al.*, "Message passing receiver for sefdm signaling over multipath channels," in *2019 IEEE VTS Asia Pacific Wireless Communications Symposium (APWCS)*. IEEE, 2019, pp. 1–5.

[11] S. Stainton *et al.*, "Neural Network Equalisation and Symbol Detection for 802.11p V2V Communication at 5.9GHz," in *2020 IEEE 91st Vehicular Technology Conference (VTC Spring)*. IEEE, 2020.

[12] S. Isam and I. Darwazeh, "Characterizing the intercarrier interference of non-orthogonal spectrally efficient FDM system," in *2012 8th International Symposium on Communication Systems, Networks & Digital Signal Processing (CSNDSP)*. IEEE, 2012, pp. 1–5.

[13] G. T. . version 8.12.0 Release 8, "Evolved universal terrestrial radio access (E-UTRA) and evolved universal terrestrial radio access network (EUTRAN); overall description; stage 2 (release 8)," April 2010.

[14] 3GPP, "LTE; Evolved Universal Terrestrial Radio Access; Physical layer procedures," 3GPP, TS 36.213, Rel. 14, v.14.2.0, Apr. 2017.

[15] W. Ozan *et al.*, "Time Precoding Enabled Non-Orthogonal Frequency Division Multiplexing," in *Proc. 30th IEEE Int. Symp. on Personal, Indoor and Mobile Radio Communications*, Sep. 2019, pp. 1–6.

[16] T. M. Schmidl and D. C. Cox, "Robust frequency and timing synchronization for ofdm," *IEEE transactions on communications*, vol. 45, no. 12, pp. 1613–1621, 1997.

[17] H. Minn *et al.*, "On timing offset estimation for OFDM systems," *IEEE Communications letters*, vol. 4, no. 7, 2000.

[18] Abdzadeh-Ziabari *et al.*, "Timing and Frequency Synchronization and Doubly Selective Channel Estimation for OFDMA Uplink," *IEEE Transactions on Circuits and Systems II: Express Briefs*, 2019.